RESEARCH ARTICLE

Hydrogenolysis of Poly(Ethylene-co-Vinyl Alcohol) and Related Polymer Blends over Ruthenium Heterogeneous Catalysts

Christine M. Oberhausen,[a,b] Jignesh S. Mahajan,[c] Jessie A. Sun,[a,b] Thomas H. Epps, III,[a,b,c] LaShanda T.J. Korley,[a,b,c] Dionisios G. Vlachos*[a,b]

[a] C.M. Oberhausen, J.A. Sun, Prof. T.H. Epps III, Prof. L.T.J. Korley, Prof. D.G. Vlachos
Department of Chemical and Biomolecular Engineering
University of Delaware
150 Academy St., Newark, DE 19716, USA
E-mail: vlachos@udel.edu

[b] C.M. Oberhausen, J.A. Sun, Prof. T.H. Epps III, Prof. L.T.J. Korley, Prof. D.G. Vlachos
Center for Plastics Innovation
University of Delaware
221 Academy St., Newark, DE 19716, USA

[c] J.S. Mahajan, Prof. T.H. Epps III, Prof. L.T.J. Korley
Department of Materials Science and Engineering
University of Delaware
127 The Green, Newark, DE, 19716, USA

Supporting information for this article is given via a link at the end of the document.

Abstract: The hydrogenolysis of polymers is emerging as a promising approach to deconstruct plastic waste into valuable chemicals. Yet, the complexity of plastic waste, including multilayer packaging, is a significant barrier to handling realistic waste streams. Herein, we reveal fundamental insights into a new chemical route for transforming a previously unaddressed fraction of plastic waste – poly(ethylene-*co*-vinyl alcohol) (EVOH) and related polymer blends – into alkane products. We report that Ru/ZrO_2 is active for the concurrent hydrogenolysis, hydrogenation, and hydrodeoxygenation of EVOH and its thermal degradation products into alkanes (C_1-C_{35}) and water. Detailed reaction data, product analysis, and catalyst characterization reveal that the in-situ thermal degradation of EVOH forms aromatic intermediates that are detrimental to catalytic activity. Increased hydrogen pressure promotes hydrogenation of these aromatics, preventing catalyst deactivation and improving alkane product yields. Calculated apparent rates of C-C scission reveal that the hydrogenolysis of EVOH is slower than low-density polyethylene. We apply these findings to achieve hydrogenolysis of EVOH/polyethylene blends and elucidate the sensitivity of hydrogenolysis catalysts to such blends. Overall, we demonstrate progress towards efficient catalytic processes for the hydroconversion of waste multilayer film plastic packaging into valuable products.

Introduction

Finding a solution to manage the growing accumulation of unrecycled plastic waste remains a pressing challenge.[1-4] The heterogeneous nature of plastic waste is one reason for such difficulty, to which multilayer films (MF) – produced at a scale of ~100 million tons/year – are a significant contributor.[5-8] MFs are complex, single-use plastics comprised of several polymers coextruded into a stacked thin film. Poly(ethylene-*co*-vinyl alcohol) (EVOH) is often included as an inner layer at up to 20 wt% to impart superior gas barrier properties for pharmaceutical and food packaging applications.[9-11] Polyolefins (POs) are primarily used for the outer layers and can constitute up to 80 wt% of the film.[12] The incompatible nature of these polar (EVOH) and non-polar (PO) polymers introduces challenges to their overall waste management. For example, mechanical recycling of MFs is not possible due to the form factor of the films, as well as the immiscibility of the various layers, which instead necessitates costly and inefficient delamination, compatibilization, or solvent-assisted processing.[6,13] Thus, post-consumer MFs are typically landfilled or incinerated.[6, 14]

Chemical deconstruction of polymers has recently emerged as a promising route to utilize plastics waste as a feedstock for fuel, lubricant, and platform chemical production.[15,16] In particular, the hydrogenolysis of plastics over heterogeneous ruthenium (Ru) catalysts has been of interest due to Ru's high activity in comparison to platinum (Pt) at relatively mild processing conditions.[17-23] Previous investigations of Ru catalysts have focused on single-component POs, such as low-density polyethylene (LDPE), high-density polyethylene (HDPE), and polypropylene (PP), and do not address the heterogeneous layers and components of MFs. As a result, investigations on the chemical conversion of EVOH and MFs are limited. Experimental and computational work has demonstrated the partial dehydration of EVOH to a non-polar solid using solid acid catalysts and solvents;[24,25] however, the direct, solvent-free deconstruction of EVOH still requires attention.

Herein, Ru/metal oxide (ZrO_2, CeO_2, TiO_2, Al_2O_3, SiO_2) catalysts are screened for the hydrogenolysis of EVOH, and Ru/ZrO_2 is selected for further study. The pathway for the deconstruction of EVOH over Ru/ZrO_2 is investigated, demonstrating significant differences from well-studied PO hydrogenolysis. Catalyst stability and deactivation are investigated to understand the impact of reaction conditions on catalytic activity over time, elucidating a significant influence of H_2 reaction pressure on activity and selectivity. Apparent rates of C-C scission indicate that the deconstruction of EVOH is ~5x slower than that of LDPE over the same catalyst. Reactions of EVOH/LDPE mixtures, used as a surrogate for MFs, suggest a nonlinear dependence of rate on the composition of films.

Results and Discussion

EVOH Characterization

EVOH is a random copolymer of ethylene and vinyl alcohol. The EVOH used in this study contains 32 wt% (42 mol%) ethylene repeat units, which translates to approximately 40/60 molar ratio of ethylene to vinyl alcohol units. ^{1}H NMR spectra of the pristine EVOH (**Figure S1**) confirm the random distribution of vinyl alcohol monomer units.[26]

Hydrogenolysis of EVOH: Reaction Data and Product Analysis

Synthesized Ru/MO_x (MO_x=ZrO_2, CeO_2, TiO_2, Al_2O_3, SiO_2) catalysts were screened for EVOH hydrogenolysis at 250 °C. Additionally, a thermal reaction (no catalyst) was tested to compare with catalytic tests, as the thermal degradation of EVOH has been reported at temperatures as low as 225 °C.[27]

The thermal reaction at 250 °C demonstrates that EVOH thermally degrades into water and waxy products with minimal formation of liquid or gas products (**Figure 1**a). Water forms *via* side-chain elimination of hydroxyl groups.[27,28] The water yield of 15.2 wt% corresponds to the elimination of 54.6 wt% of the initial EVOH hydroxyl side chains. The molten polymer may form a six-membered transition state and undergo backbone chain scission, resulting in shorter-chain waxy products.[27,28] Attenuated total reflectance - Fourier transform IR (ATR-FTIR) spectra of the thermal wax products show significant peaks at 3350 cm^{-1}, 2920 and 2850 cm^{-1}, and 1710 cm^{-1}, corresponding to O-H, CH_2 symmetric and asymmetric, and C=O stretches, respectively (**Figure 1**d).[29,30] The C=O stretching peak has a broad shoulder at lower wavenumbers (1700-1600 cm^{-1}), indicating a multitude of additional C=O and C=C species at lower concentrations (**Figure 1**d)[30,31] The formation of carbonyl moieties is consistent with previous findings on the thermal degradation of vinyl alcohol polymers, which report keto-enol tautomerization of C=C moieties.[28,32] Further, ^{1}H NMR spectra of the thermal wax indicate unsaturated species, as shown by peaks in the 4.5-6.0 ppm and 6.0-8.5 ppm shift range, corresponding to unsaturated olefin and aromatic moieties, respectively (**Figure 1**c). ATR-FTIR and ^{1}H NMR spectra of the thermal solid residue indicate moieties similar to those of the wax (**Figure S2**a,**Figure S2**b). Gel permeation chromatography (GPC) of the thermal wax (**Figure 1**e) shows a broad molecular weight distribution from 800-1,000,000 g/mol (C_{50}-$C_{70,000}$), demonstrating that both chain scission and chain growth *via* cross-linking of unsaturated moieties occur in the absence of a catalyst.[33]

The addition of Ru/ZrO_2 and Ru/CeO_2 hydrogenolysis catalysts drastically increases the degree of C-C scission in comparison to the thermal baseline, achieving nearly complete deconstruction of EVOH in just 2 h with an 80:1 polymer-to-catalyst ratio (**Figure 1**a). Other catalysts show markedly lower activity, producing >50 wt% solid yield (**Figure 1**a).

It is hypothesized that the Ru/MO_x catalysts act on the thermally degraded EVOH, in addition to directly catalyzing the C-C scission of the pristine EVOH itself. Wax is the major product formed with Ru/ZrO_2 and Ru/CeO_2. GPC traces of the waxes indicates a molecular weight distribution of 200-20,000 g/mol (~C_{15}-C_{1400}), which is narrowed and shifted to lower values than the thermal wax (**Figure 1**e). The intensity of ^{1}H NMR spectra peaks in the 4.5-8.5 ppm range for the waxes is reduced in comparison to the thermal baseline, indicating that Ru/MO_x catalysts partially hydrogenate polyenes (unsaturated olefinic and aromatic moieties) that form *via* thermal degradation (**Figure 1**c).[34,35] Peaks on the ATR-FTIR spectra at 1700-1600 cm^{-1} are absent, and the peak at 1710 cm^{-1} has reduced intensity, indicating that the C=C and C=O moieties are decreased, respectively (**Figure 1**d). This observation provides additional evidence for the catalytic hydrogenation of unsaturated moieties. The reactions over Ru/ZrO_2 and Ru/CeO_2 show slightly increased water yields in comparison to thermal decomposition (**Figure 1**a), suggesting that water forms *via* catalytic hydrodeoxygenation (HDO) over Ru/MO_x in addition to thermal side-chain elimination.[36] The Ru/ZrO_2 and Ru/CeO_2 catalysts also promote the deconstruction of wax into liquid products. The liquid contains alkanes, alcohols, ketones, and aromatic species (**Figure 1**b). Furthermore, Ru/ZrO_2 and Ru/CeO_2 catalyze the deconstruction of wax and liquid species into saturated hydrocarbon gas products (**Figure 1**b). Ru/TiO_2, Ru/Al_2O_3, and Ru/SiO_2 have lower activity for EVOH hydrogenolysis, shown by significantly higher solid yields, and lower yields of wax, liquid, and gas products (**Figure 1**a).

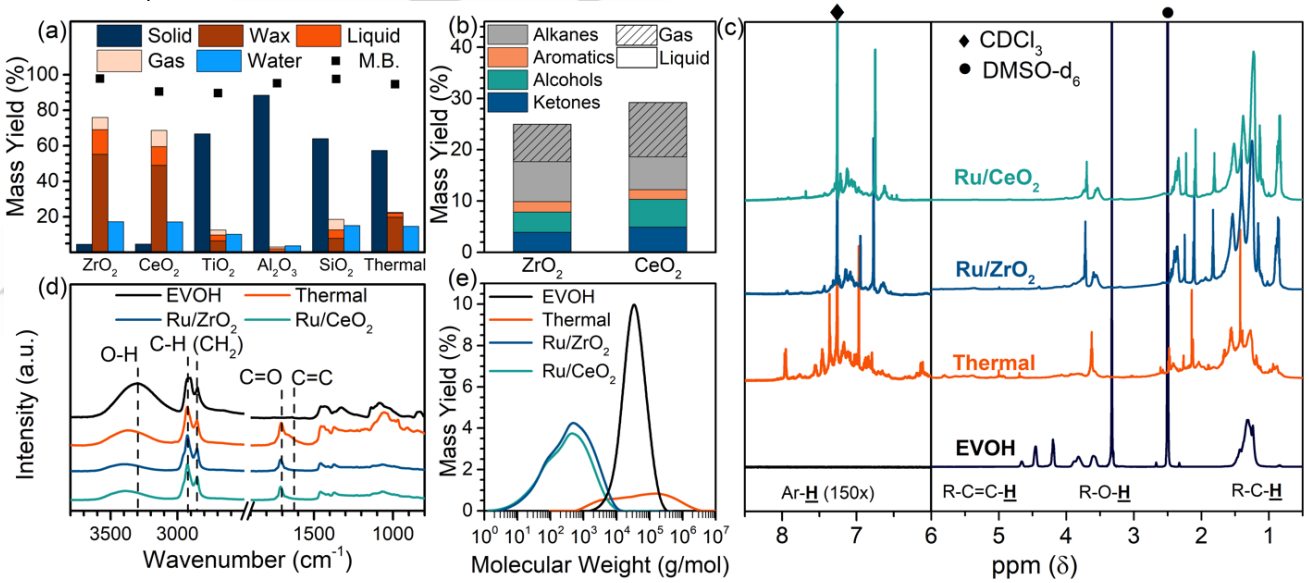

Figure 1. Ru/MO_x catalyst screening for EVOH hydrogenolysis. (a) Product phase data. (b) Liquid and gas product yields for select catalysts. (c) ^{1}H NMR spectra (the y-axis of the 8.5-6.0 ppm region is magnified 150x), (d) ATR-FTIR spectra, and (e) GPC molecular weight distribution traces of select wax products in comparison to pristine EVOH. Reaction conditions: 250 °C, 30 bar H_2, 2 h, 2.0 g EVOH, 80:1 polymer-to-catalyst ratio (excluding thermal blank), 5 wt% Ru loading on metal oxide supports.

Of the catalysts tested, Ru/ZrO_2 was chosen for further investigation due to its high activity, and lower gas selectivity in comparison to Ru/CeO_2.

Reactions were carried out at 250 °C, as this achieves a balance between catalytic activity of Ru/ZrO_2 and the thermal degradation of EVOH. To illustrate this, EVOH hydrogenolysis over Ru/ZrO_2 was tested at varying temperatures and compared to thermal baselines (no catalyst) at the same conditions (**Figure S3**a). Lower temperature (225 °C) demonstrates significantly decreased catalytic activity, shown by higher solid yields, likely requiring extended reaction times to achieve high conversions (**Figure S3**b). Conversely, at higher temperatures, EVOH undergoes more severe thermal degradation, resulting in higher concentrations of aromatics (**Figure S3**c, **Figure S3**d). Additionally, increased temperature (275 °C) significantly increases the yield of undesirable methane (**Figure S3**c).

A series of time-dependent reactions at 250 °C were carried out to propose a reaction network for the hydrogenolysis of EVOH over Ru/ZrO_2 at varying reaction pressures. At 30 bar H_2, initial EVOH hydrogenolysis is fast. 20 wt% of the starting polymer is deconstructed during the ramping time to minor yields of wax, liquid, gas, and water products (**Figure 2**a). The remaining solid has a narrower molecular weight distribution in comparison to pristine EVOH (**Figure S4**a). Peaks at 3300 cm^{-1}, 3000-2850 cm^{-1}, and 1710 cm^{-1} on the ATR-FTIR spectra of the 0 h wax indicate O-H, C-H, and C=O stretching peaks, respectively (**Figure 2**b). Additionally, a minor shoulder from 1700-1650 cm^{-1} indicates small concentrations of C=O and C=C moieties (**Figure 2**d). ^{1}H NMR spectra of the 0 h wax show considerable peaks in the 9.0-7.4 and 7.4-6.5 ppm range, indicative of both polyaromatic and monoaromatic species, respectively (**Figure 2**c).[37,38] After 1 h, there is a slight increase in wax, liquid, and gas yields (**Figure 2**a). The wax has reduced O-H, C=O, and C=C concentrations in comparison to the 0 h wax, as shown by the reduction in intensity of these respective peaks in the ATR-FTIR and ^{1}H NMR spectra (**Figure 2**b, **Figure 2**c). The liquid and gas products are mostly alkane species (**Figure 2**d). By 2 h of reaction, the solid is almost completely deconstructed, and the maximum wax and liquid yields are achieved. The molecular weight distribution of the wax is 100-5,000 g/mol (C_8-C_{350}) (**Figure 2**e). ATR-FTIR spectra show decreased intensity of O-H and C=O stretching peaks, indicating HDO of the wax products, and the peak from 1700-1650 cm^{-1} is diminished, indicating a reduced concentration of C=C moieties (**Figure 2**b). A reduction in unsaturated aromatics is also evident from the reduced peak intensity from 8.5-6.0 ppm in ^{1}H NMR spectra of the 2 h wax (**Figure 2**c). In contrast, the liquid products at 2 h have an increased yield of aromatics, ketones, and alcohols, with a combined oxygenates yield of 14.5 wt% (**Figure 2**d).

Between 2 and 16 h, ATR-FTIR spectra show decreased O-H and C=O stretching peak intensities, indicating further HDO of the wax products (**Figure 2**b). Similarly, HDO is observed in the liquid fraction, as alcohol liquid yields decrease, and majority alkane liquid products are formed by 16 h (**Figure 2**d). The liquid fraction is deconstructed into gas species over time (**Figure 2**a); however, the wax yield remains approximately constant, at 34 wt%. Beyond 8 h of reaction, there is no significant change in yields, compositions, or molecular weight distributions of the products. The only minor change is increased aromatic concentrations in the wax and liquid, shown by increased peak intensities at 8.5-6.0 ppm in the ^{1}H NMR spectra of the wax and increased aromatic yield (~1.5 wt%) in the liquid products, with a qualitative increase in polyaromatics by 16 h of reaction (**Figure 2**c). This lack of change in wax, liquid, and gas yields suggests that there is a complete loss in C-C scission activity after 8 h of reaction at 30 bar H_2. The hydrogenolysis of EVOH over Ru/ZrO_2 consumes a considerable quantity of H_2 (**Figure S5**a, **Figure S5**b), and it is known that the rate of C-C scission for long-chain hydrocarbon species is highly pressure-dependent, with lower H_2 pressures leading to decreased activity. For this reason, a semi-batch reaction was tested for the hydrogenolysis of EVOH at 30 bar H_2. The semi-batch reaction showed no improvement in deconstruction in comparison to the batch reaction, manifested by identical phase yields and similar carbon number distribution of liquid and gas species (**Figure S6**). This behavior suggests that the loss in activity can be attributed to a change in the catalyst, rather than a reduction in H_2 pressure.

Time-dependent reactions at increased pressure (60 bar H_2) lead to notable differences. Initial deconstruction is faster, with 37 wt% of the initial solid deconstructed during ramp time alone (**Figure 3**b), forming significant yields of wax, liquid, gas, and water products (**Figure 3**a). The wax at 0 h contains hydroxyl and carbonyl sidechains, as indicated by O-H and C=O stretching peaks on the ATR-FTIR spectra (**Figure 3**b), but at relatively lower concentrations than at 30 bar H_2. Additionally, the ^{1}H NMR spectra of the wax at 0 h indicate primarily alkane moieties in the 0.5-2.5 ppm region, with minor concentrations of aromatics (6.0-8.5 ppm). Peaks are absent between 2.5-6.0 ppm, indicating minimal concentrations of unsaturated olefinic moieties (**Figure 3**c). The liquid and gas are primarily alkanes, with a small fraction of ketones (**Figure 3**d). Minimal aromatic species are evidenced in the wax and liquid products. Evidently,

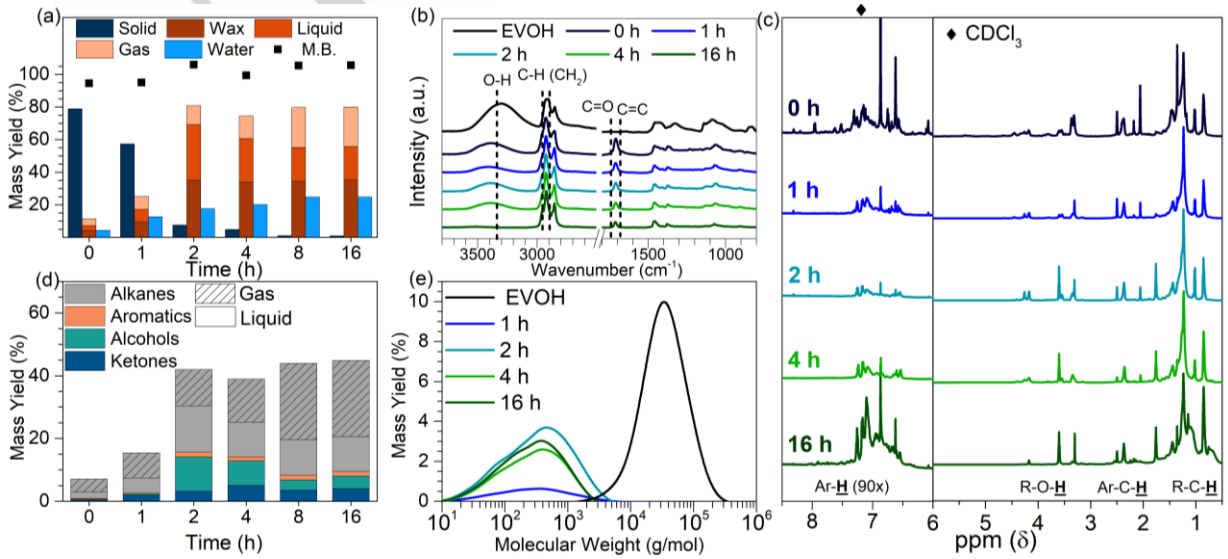

Figure 2. Hydrogenolysis of EVOH over Ru/ZrO_2 at 30 bar H_2. (a) Product phase data. (b) ATR-FTIR spectra and (c) ^1H NMR spectra (the y-axis of the 8.5-6.0 ppm region is magnified 90x) of wax products. (d) Product yields of liquid and gas products. (e) Molecular weight distribution traces of wax products. Reaction conditions: 250 °C, 30 bar H_2, 2.0 g EVOH, 40:1 polymer-to-catalyst ratio, 5 wt% Ru on ZrO_2, varying time.

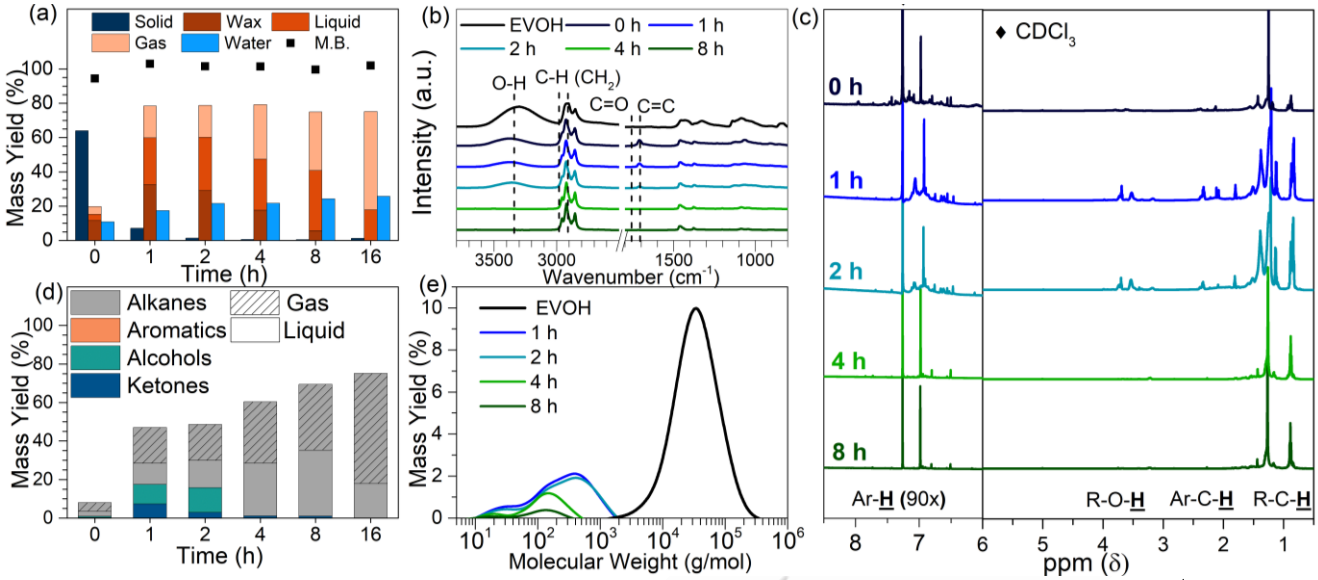

Figure 3. Hydrogenolysis of EVOH over Ru/ZrO_2 at 60 bar H_2. (a) Product phase data. (b) ATR-FTIR spectra and (c) ^1H NMR spectra (the y-axis of the 8.5-6.0 ppm region is magnified 90x) of wax products. (d) Product yields of liquid and gas products. (e) Molecular weight distribution traces of wax products. Reaction conditions: 250 °C, 60 bar H_2, 2.0 g EVOH, 40:1 polymer-to-catalyst ratio, 5 wt% Ru on ZrO_2, varying time.

hydrogenation is promoted at increased H_2 pressures, resulting in higher yields of saturated products in comparison to 30 bar H_2 reactions. In just 1 h of reaction, over 90 wt% of the solid is deconstructed to lower molecular weight products. The oxygenated moieties increase in the wax and liquid fractions at 1 h (**Figure 3**d, **Figure 3**c). The wax molecular weight distribution is narrower than at 30 bar H_2, with a range of 100-2,000 g/mol (C_8-C_{140}) (**Figure 3**e).

Between 1-2 h of reaction, the phase yields remain unchanged (**Figure 3**a), and the wax products maintain a stable molecular weight distribution; minimal C-C scission is observed (**Figure 3**e). Rather, the unsaturated carbonyl moieties are hydrogenated, shown by a decrease in C=O and an increase in O-H peaks in the ATR-FTIR spectra of the waxes, with a concomitant decrease in ketones yield and increase in alcohols yield in the liquid product (**Figure 3**b, **Figure 3**d). Hydrogenation of aromatic moieties in the wax also is evident, shown by a reduction in peak intensities from 6.0-8.5 ppm in the ^1H NMR spectra (**Figure 3**c).

After 2 h of reaction, C-C scission dominates, displayed by decreased wax yields with narrowed and shifted molecular weight distributions (**Figure 3**a, **Figure 3**e). This trend sharply differs from the plateau in wax yields observed at the lower hydrogen pressure. At 60 bar H_2, oxygenated species undergo HDO to form solely saturated hydrocarbon wax, liquid, and gas products, shown by the significantly decreased yields of oxygenated liquid products (**Figure 3**d) and the absence of O-H and C=O stretching peaks in the ATR-FTIR spectra of the wax by 4 h (**Figure 3**b). From 4 to 16 h of reaction, C-C scission continues, leading to the progressive deconstruction of wax into liquid and then gas alkane products (**Figure 3**a, **Figure 3**d).

Time-dependent reactions show that pressure profoundly impacts catalytic activity and product composition. Lower pressures favor higher concentrations of unsaturated ketones and aromatics, whose hydrogenation is slow. The wax products forming at short times do not deconstruct with extended reaction time, indicating a loss of catalytic activity. In contrast, increased H_2 pressure preserves catalytic activity over the course of the reaction and forms high yields of saturated hydrocarbon products.

The data suggest that the deconstruction of EVOH over Ru/ZrO_2 proceeds through three distinct stages (**Scheme 1**). Stage 1 is the simultaneous thermal degradation and catalytic C-C scission of initial high-MW solid to form primarily mid-MW wax and liquids with unsaturated and oxygenated moieties, with minor yields of gas products. Once the solid is fully deconstructed, Stage 2 entails the hydrogenation and HDO of mid-MW products (wax and liquids) with minimal C-C scission to produce mid-MW saturated hydrocarbon species. Finally, once hydrogenation and HDO are complete, C-C scission dominates, leading to the deconstruction of mid-MW waxes into small-MW saturated liquid and gas alkanes (C_1-C_{35}). At 30 bar H_2, the catalyst deactivates during Stage 2 (hydrogenation and HDO), and therefore, Stage 3 (C-C scission) production of saturated hydrocarbon liquids and gases, never occurs. Instead, a complex mixture of waxy aromatics, ketones, alcohols, and alkanes remains at the end of reaction. In contrast, reactions at 60 bar H_2 proceeds through all three stages, resulting in 'deep' hydrogenolysis of EVOH to form saturated alkane products.

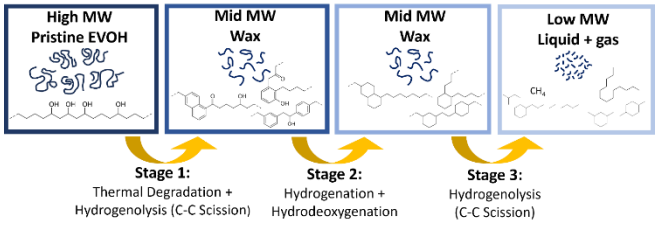

Scheme 1. Proposed pathway of EVOH hydrogenolysis over Ru/ZrO_2. 'MW' = molecular weight, of the product species.

Spent Catalyst Characterization and Regeneration

The spent catalysts of reactions at 30 bar H_2 were characterized to confirm catalyst deactivation. Structural changes were

investigated using TEM and XRD. Qualitative inspection of the TEM of the spent catalyst after 16 h of reaction at 30 bar H_2 shows no significant change in particle size in comparison to those of fresh Ru/ZrO_2 (**Figure S7**c, **Figure S8**c). The absence of Ru peaks on XRD diffractograms at all reaction times suggests that the Ru particle sizes remain <5 nm throughout the reaction, indicating minimal sintering (**Figure S9**a&b).[39] The ZrO_2 structure is monoclinic with a minor tetragonal crystal structure.[40,41]

Upon confirming a stable catalyst structure, we hypothesized that adsorbed species on the catalyst surface could cause catalyst deactivation. TGA quantified the amount (wt%) of surface deposits as a function of time (**Figure 4**a). DSC of surface species indicates the 'hardness' of adsorbed species, with higher temperatures of removal correlated with higher molecular weight carbonaceous species and stronger adsorption (**Figure 4**b).[42] Fresh Ru/ZrO_2 shows <1 wt% removal of species at near ambient temperatures, suggesting its minimal surface species. After 8 h of reaction, the spent catalyst has a small quantity of deposits (~4 wt%). DSC curves demonstrate that the oxidative removal of the adsorbed species is complete by 250 °C, indicating weakly adsorbed species that can likely be removed at reaction conditions in a reductive environment. The 16 h spent catalyst loss is significant (~15 wt%), exhibiting a much higher concentration of carbonaceous deposits. The DSC traces show the most intense peak at 250 °C, associated with lower molecular weight species. Additional peaks at 400 °C and 525 °C indicate strongly adsorbed, higher molecular weight species that cannot be removed at reaction temperatures. These species are hypothesized to cause deactivation, warranting closer investigation.

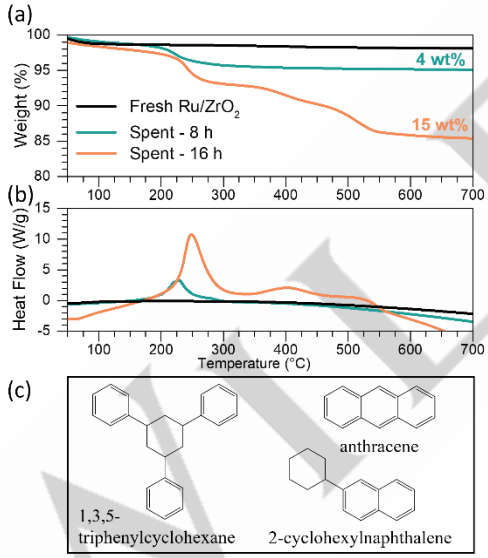

Figure 4. Characterization of spent catalysts. (a) TGA thermograms of fresh and spent Ru/ZrO_2. (b) DSC thermograms of fresh and spent Ru/ZrO_2. (c) Examples of polyaromatic species identified *via* GC-MS of CH_2Cl_2 solution following Soxhlet extraction of spent Ru/ZrO_2 (**Figure S10**).

Soxhlet extraction of spent Ru/ZrO_2 catalysts after 16 h of reaction was completed to extract adsorbed species from the catalyst surface and pores. Polyaromatics, such as 1,3,5-triphenylcyclohexane, 2-cyclohexylnaphthalene, and anthracene, were identified in the extraction solvent (**Figure 4**c). It is possible that higher molecular weight species were also removed from the catalyst surface, but they could not be detected using GC-MS.

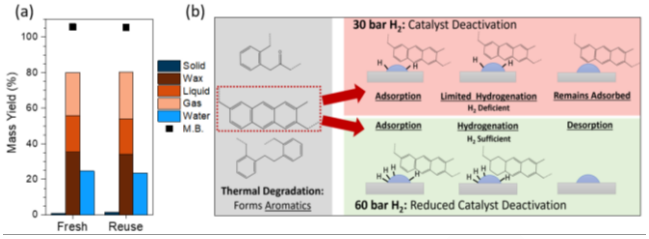

Figure 5. Catalyst deactivation and regeneration. (a) Reuse test. Reaction conditions: 250 °C, 30 bar H2, 16 h, 2 g EVOH, 40:1 polymer-to-catalyst ratio, 5 wt% Ru on ZrO2. (b) Proposed scheme showing the influence of pressure on catalyst deactivation.

The spent catalyst was regenerated to remove such polyaromatic species. Ru/ZrO_2 catalyst collected after 16 h reaction at 30 bar H_2 was reduced under H_2 flow at 300 °C for 2 h. The freshly reduced catalyst was then reused, and complete regeneration was found, shown by identical yields of wax, liquid, and gas products (**Figure 5**a). It is hypothesized that such catalyst regeneration occurs through the hydrogenation of adsorbed polyaromatic species. Once saturated, the resulting polycyclic species have decreased binding strength to the catalyst and can desorb by 300 °C.[43,44] During reaction, the low solubility of H_2 gas in polymer melts may severely limit the availability of H_2 on the catalyst surface, slowing the hydrogenation of these polyaromatics.[45,46] Thus, at 30 bar H_2, insufficient hydrogenation allows subsequent aromatization, leading to polyaromatics and catalyst deactivation. To overcome this, increased H_2 pressure improves the solubility of H_2 in the polymer melt. This improved hydrogen accessibility promotes hydrogenation and mitigates the deposition of catalyst-deactivating polyaromatic species (**Figure 5**b). Thus, sufficient hydrogen can promote the *in-situ* hydrogenation and removal of polyaromatic surface species, preserving catalytic activity.

Comparison of EVOH and LDPE Hydrogenolysis

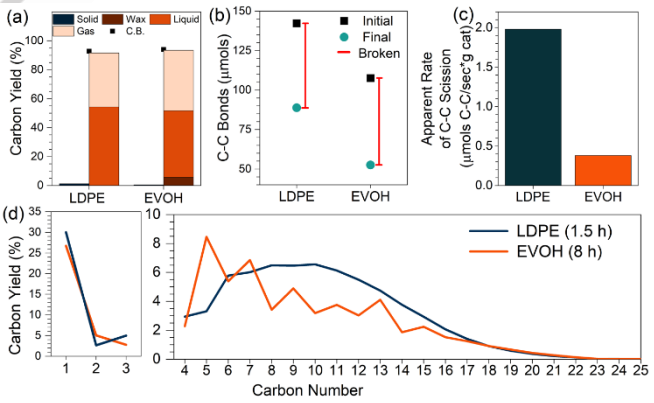

Figure 6. LDPE and EVOH hydrogenolysis comparison. (a) Phase yields and (b) number of C-C bonds present at the beginning and end of the reaction, with the red line representing the µmols of C-C bonds broken. (c) Calculated apparent rates of C-C scission for hydrogenolysis of LDPE and EVOH. (d) Carbon number distributions for hydrogenolysis of EVOH and LDPE. Reaction conditions: 250 °C, 60 bar H_2, 2.0 g polymer, 40:1 polymer-to-catalyst ratio, 5 wt% Ru on ZrO_2, (LDPE: 1.5 h, EVOH: 8 h).

The hydrogenolysis of EVOH and LDPE over the Ru/ZrO_2 catalyst was compared at identical reaction conditions, with reaction time varied to achieve identical product distributions (**Figure 6**a) and a similar number of C-C bonds broken (**Figure 6**b). Interestingly, EVOH requires 8 h compared to 1.5 h for LDPE to reach similar distribution of liquid and gas products (**FigureFigure 6**d). These

reaction systems with highly viscous polymers are likely to be under mass-transfer controlled regimes. Therefore, apparent reaction rates are calculated, which include the effect of transport phenomena. The apparent C-C scission rate for EVOH hydrogenolysis is 5x lower than that of LDPE (**Figure 6**c), even at an elevated H_2 pressure (60 bar). Although catalyst deactivation is minimal at these higher pressures, the competing hydrogenation of aromatics and HDO of ketones and alcohols may contribute to lower observed C-C scission rates.[47,48]

Hydrogenolysis of EVOH/LDPE Mixtures

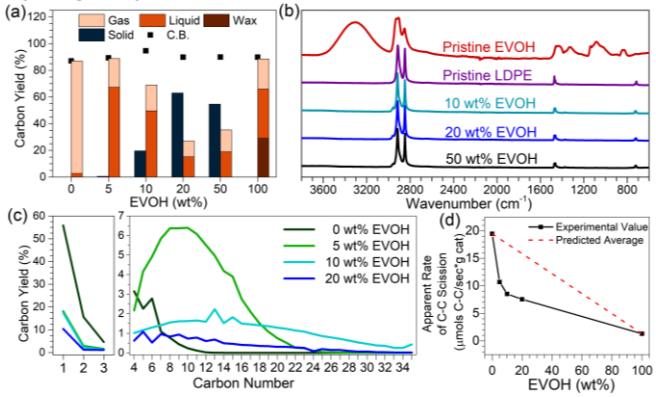

Figure 7. Hydrogenolysis of LDPE/EVOH mixtures and individual polymers at 60 bar H_2. (a) Phase yields. (b) ATR-FTIR spectra of solid residues. (c) Carbon number distribution of gas and liquid alkane products. (d) Apparent rates of C-C scission for varying ratios of EVOH and LDPE. Reaction conditions: 250 °C, 60 bar H_2, 2 h, 2.0 g total polymer, 40:1 polymer-to-catalyst ratio, 5 wt% Ru on ZrO_2.

Next, the hydrogenolysis of EVOH/LDPE mixtures, as surrogate for MFs, was conducted with varying wt% of EVOH at 60 bar H_2. Adding EVOH slows down the catalytic deconstruction of EVOH/LDPE mixtures. With 5 wt% EVOH, the solid is fully deconstructed, but the gas yield decreases, and the liquid yield increases in comparison to converting LDPE alone, indicating that the deconstruction of LDPE is significantly slowed with the inclusion of EVOH (**Figure 7**a). Further increasing the fraction of EVOH increases solid yields and decreases liquid and gas yields. ATR-FTIR spectra of solid residues resemble pristine LDPE, indicating that there is minimal oxygen (O-H or C=O) present in the remaining solid. (**Figure 7**b). Additionally, no wax products are observed; rather, lighter molecular-weight liquid and gas alkane products are seen. This result indicates that the EVOH portion of the mixtures has proceeded through all stages of hydrogenolysis (i.e. deep hydrogenolysis), shown in Scheme 1, to form saturated hydrocarbon liquid and gas products.

Apparent C-C scission rates were calculated for reactions of mixtures with 5-20 wt% EVOH with the reaction time varied to achieve identical yields of solid, liquid, and gas products between each (**Figure S11**). These reactions highlight that longer reaction times are required to deconstruct mixtures with increasing amounts of EVOH, and the apparent rate of C-C scission decreases with increasing wt% EVOH. Additionally, apparent rates for mixtures significantly deviate from the predicted weighted average of the two polymers (**Figure 7**d). There are multiple factors that may give rise to this deviation. For example, probe reactions with LDPE demonstrate that the presence of bulky aromatic species, such as butyl benzene and naphthalene, from EVOH deconstruction can significantly hinder LDPE hydrogenolysis (**Figure 8**a, **Figure 8**b). This work illustrates that extending reaction time is one simple method to overcome these challenges and achieve full deconstruction of LDPE/EVOH mixtures. Yet, this area deserves more in-depth investigation in the future.

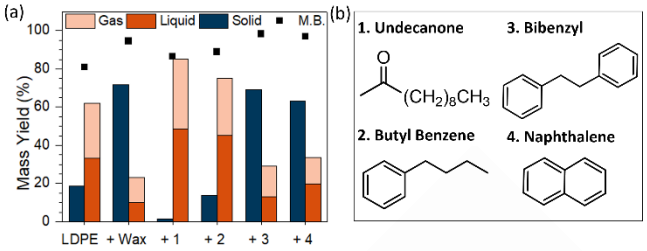

Figure 8. Reaction data for LDPE hydrogenolysis over Ru/ZrO_2 with the addition of probe molecules. (a) Reaction data. (b) Molecular structures of probe molecules. Reaction Conditions: 250 °C, 30 bar H2, 2 h, 2.0 g LDPE, 50 mg probe molecule, 40:1 polymer to catalyst ratio. The wax product collected after 1 h of EVOH hydrogenolysis at 250 °C, 30 bar H_2 over Ru/ZrO_2.

Conclusion

We demonstrated that Ru/ZrO_2 is an active catalyst for simultaneous EVOH hydrogenolysis, hydrodeoxygenation (HDO), and hydrogenation of polyenes and subsequent deconstruction products. A complete deconstruction of EVOH into wax, liquid, and gas products was achieved in just 2 h. Thermal degradation proceeds concurrently at typical hydrogenolysis conditions, producing aromatics that are detrimental to catalyst activity. Detailed product analysis and catalyst characterization revealed that increased hydrogen pressure promotes aromatics hydrogenation, minimizing catalyst deactivation and enabling full deconstruction of EVOH into lower molecular weight liquid and gas products. Upon full deconstruction of EVOH (8 h), the sole products are C_1-C_{35} alkanes and water, with a maximum yield of 35 wt% C_6-C_{36} alkanes. The C-C scission rate in EVOH over Ru/ZrO_2 is ~5x lower than that of LDPE, presumably due to the formation of polyenes and aromatics that are slowly hydrogenated. Mixtures of EVOH and LDPE, tested as surrogates for real MFs, react slower than the predicted weighted average of the two individual polymers. Extending reaction time partially alleviates this problem.

Thus, this work highlights the difficulties in achieving efficient hydrogenolysis of EVOH and EVOH-containing polymer blends and provides routes to overcoming these challenges. As a result, fundamental insights were revealed that are critical to future investigations on the chemical deconstruction of real multilayer films. Additionally, this work elucidates the sensitivity of previously investigated hydrogenolysis catalysts to heterogeneous polymer blends, ultimately emphasizing the need for a more tailored approach to designing efficient catalytic processes for the hydroconversion of mixed plastic waste streams.

Experimental Methods

Feedstocks

Poly (ethylene-*co*-vinyl alcohol) [EVOH, 32 wt% ethylene, weight-average molecular weight (M_w) ~74 kDa, number-average molecular weight (M_n) ~43 kDa] and low-density polyethylene [LDPE, M_w ~76 kDa, M_n ~39.5 kDa] were purchased from Sigma Aldrich. Molecular weight distribution traces of the pristine polymers can be found in the Supporting Information (**Figure S12**a, **Figure S12**b). The polymers were used as received.

Catalyst Preparation

Ru supported on zirconia was synthesized using wetness impregnation. $ZrO_x(OH)_{4-2x}$ was made by hydrolysis of zirconyl chloride octahydrate ($ZrOCl_2 \cdot 8H_2O$, Aldrich, 98%) solution using ammonium hydroxide (NH_4OH, Aldrich, 28–30 wt% in H_2O), as reported previously.[49] The resulting ZrO_2 was then impregnated with ruthenium(III) nitrosyl nitrate solution ($Ru(NO)(NO_3)_x(OH)_{3-x}$, Aldrich, 1.5 wt% Ru) to achieve 5 wt% nominal metal loading. The resulting slurry was dried at 110 °C for 12 h and then subjected to a 2 h reduction treatment, carried out in a tubular reactor using 50% H_2/He in 100 mL/min total gas flow at 300 °C. 5 wt% Ru supported on other metal oxides were prepared by the same method (CeO_2: Alfa Aesar, calcined at 650 °C. Al_2O_3: Sasol Pural, calcined at 650 °C. SiO_2: Sigma Aldrich (<63 μm), calcined at 650 °C. TiO_2: US Research Nanomaterials, < 5 nm, calcined at 450 °C). Ru supported on metal oxide catalysts are referred to as Ru/MO_x.

Hydrogenolysis Experiments

The appropriate ratio of freshly reduced Ru/MO_x and 2.0 g of polymer feedstock was mixed with a vortex mixer and added to a 50 mL Parr batch reactor with a PTFE stir bar. The Parr reactor was sealed, purged 5 times with 10 bar H_2, and then charged with H_2 to the desired reaction pressure. The reactor was then ramped to reaction temperature (250 °C), with stirring turned on (500 rpm) once it reached the polymer melting temperature (EVOH = 180 °C, LDPE = 145 °C). The reaction was maintained at reaction temperature for specified time intervals, then quenched in an ice bath and cooled to below 5 °C prior to product extraction. Semi-batch reactions were completed using the same procedure as outlined above, but with H_2 replenished at specified time intervals during reaction. Probe reactions with LDPE were carried out following the same procedure, except 50 mg of the probe molecule was mixed with the freshly reduced catalyst and polymer feedstock prior to reaction. Triplicates of one reaction were carried out to verify the repeatability of hydrogenolysis experiments, and a range of error less than ±3 wt% yield was confirmed for the reaction phase data (**Figure S13**).

Product Analysis

Product Extraction and Quantification. Gas products (C_1-C_5) from the headspace of the cooled reactor were collected in a 1L Tedlar bag and quantified with gas chromatography - flame ionization detector (GC-FID) using an Agilent CP Volamine column calibrated with alkane standards. Soluble liquid (C_6-C_{35}) and wax (C_{36}-C_{299}) and insoluble solid (~C_{300+}) products were extracted from the reactor vessel using tetrahydrofuran (THF, Sigma Aldrich, 99.90%, contains 250 ppm BHT) and octacosane (O0002, TCI) standard. The liquid and wax products were separated from solid products *via* filtration (1001-090, Whatman filter paper). The solid was dried overnight. Water content of the extracted solution was quantified using a Mettler Toledo V20 Karl Fischer volumetric titrator (KF, Methanol dry, Composite-5, Honeywell Hydranal). Liquid products were identified with gas chromatography – mass spectrometry (GC-MS) using an Agilent DB-1 column and quantified with GC-FID equipped with an Agilent HP-1 column, which was calibrated with alkane, alcohol, ketone, and aromatic standards. Liquid products, water, and THF were removed with a rotary evaporator to isolate the wax products. Solid and wax products were quantified gravimetrically.

Balances and Yields. Mass and carbon balances, as well as the respective yields for each product fraction, were calculated using the following equations:

$$Mass\ balance\ (M.B.) = \frac{m_{solid} + m_{wax} + m_{liquid} + m_{gas} + m_{water}}{m_{initial}}$$

$$Mass\ Yield, Y_{m,i} = \frac{m_i}{m_{initial}}$$

$$Carbon\ balance\ (C.B.) = \frac{n_{c,solid} + n_{c,liquid} + n_{c,gas}}{n_{c,initial}}$$

$$Carbon\ Yield, Y_{c,i} = \frac{n_{c,i}}{n_{c,initial}}$$

The solid and wax masses were measured gravimetrically, the liquid and gas masses were calculated from the carbon yields determined with GC-FID, and the water mass was determined with KF titration.

A carbon balance is used only for LDPE reactions, in which products are exclusively solid, liquid, and gas, or for high conversion EVOH reactions with solely gas and liquid products. For both cases, the moles of carbon of non-solid products were determined using GC methods. The carbon yield of solid residues from LDPE reactions was approximated from the stoichiometry of pristine LDPE.

Molecular Weight Distributions. The molecular weight distributions of the wax and solid products were determined using gel permeation chromatography (GPC). The molecular weight distribution of the wax was determined with GPC (Styragel HR 4, HR 3, and HR 0.5 columns in tandem; dimensions 4.6 × 300 mm) using THF (without stabilizer, Sigma Aldrich) as mobile phase (0.3 mL/min flow rate) and a Waters 2414 refractive index detector (RID). The retention time was calibrated using a Polystyrene (PS) Standards Kit (Waters, WAT058931).

The yield distribution functions for wax products were calculated by:

$$mass\ yield, y_{m,i} = Y_{m,wax} * H_N(t_R) = Y_{m,wax} * \frac{H(t_R)}{\int H(t_R) dt_R}$$

wherein $Y_{m,wax}$ is the mass yield of wax, H_N is the normalized RID response calculated using the raw refractive index (RI) response (H) as a function of the retention time (t_R), normalized by the total RI response peak area of the eluted sample.

The methodology for acquiring molecular weight distributions of solid polymers and post-reaction solid residues can be found in the Supporting Information.

C-C Bond Calculations. The apparent rate of C-C scission was calculated using the starting number-average molecular weight of the polymers and the resulting product distributions. The full methodology for C-C bond calculations can be found in the Supporting Information.

Fourier-Transform Infrared Spectroscopy. Attenuated total reflectance Fourier-transform IR (ATR-FTIR) spectra were recorded on a Thermo Nicolet NEXUS 870 FTIR (Thermo Fisher Scientific) equipped with a potassium bromide detector and Smart Omni ATR accessory in the 4000-400 cm^{-1} range with 32 scans collected at a resolution of 4 cm^{-1}.

Nuclear Magnetic Resonance Analysis. ^1H nuclear magnetic resonance (^1H NMR) spectra of wax products were recorded at 25 °C on an Avance III 400 MHz NMR spectrometer (Bruker). A sample (~100 mg) was dissolved in 700 μL of $CDCl_3$ (Sigma Aldrich, 99.8 atom% D). ^1H NMR spectra of pristine EVOH were

recorded in the same manner, except with deuterated dimethyl sulfoxide (DMSO-d_6, Sigma Aldrich, 99.5 atom% D) used as the solvent. Data processing was performed using the Mestrelab Research software (mNOVA).

Catalyst Characterization

X-Ray Fluorescence (XRF). Ruthenium loading was estimated on a Rigaku Supermini 200 WDXRF in a He atmosphere (**Table S1**). *N_2 Sorption.* Porosity and surface area were investigated by N_2 sorption at −196 °C on a Micromeritics ASAP 2020 instrument. Before measurements, the samples were degassed at 300 °C for 3 h **(Table S1)**.

X-Ray Diffraction (XRD). The X-ray diffraction patterns of fresh and spent Ru/ZrO_2 catalyst samples were measured on a Bruker D8 diffractometer with a 0.05° 2θ, 1s per point, using Cu Kα radiation (λ = 1.54 Å).

Thermogravimetric Analysis/Differential Scanning Calorimetry. Thermogravimetric analysis (TGA) and differential scanning calorimetry (DSC) of fresh and spent catalysts were conducted on a Q600 TGA/DSC instrument (TA Instruments) in flow of air (50 mL/min) in the range of 25 °C to 700 °C with a 20 °C/min heating rate.

Soxhlet Extraction. Spent catalysts were isolated from polymer residues by dissolving polymer in solvent and filtering the solution. Isolated spent catalysts were then subjected to reflux of dichloromethane (CH_2Cl_2, Thermo Fisher, 99.9%) at 70 °C for 16 h. The resulting solvent extract was then analyzed with GC-MS (Agilent DB-1 column) to identify extracted species.[50]

Transmission Electron Microscopy. Images of fresh and spent Ru/ZrO_2 catalysts were obtained with transmission electron microscopy (TEM) using a field emission gun transmission electron microscope (JEOL, JEM2010F) with an accelerating voltage of 200 kV. Aberration Corrected High-angle Annular Dark Field Scanning/Transmission Electron Microscopy (HAADF-STEM) was performed on a JEOL NEOARM operating at 200 kV. Ru/ZrO_2 samples were dispersed in an ethanol solution and deposited on copper grids containing lacey carbon (Ted Pella, Inc. cat.#01881).

Acknowledgements

CMO, THE, and DGV were supported by a Project Award Agreement from the National Institute for Innovation in Manufacturing Biopharmaceuticals (NIIMBL) and financial assistance award from the U.S. Department of Commerce, National Institute of Standards and Technology. JAS, THE, and LTJK were supported by the Center for Plastics Innovation (CPI), an Energy Frontier Research Center (EFRC) supported by the U.S. Department of Energy (DOE), Office of Science, Office of Basic Energy Sciences grant number DE-SC0021166. JSM was supported by the National Science Foundation (NSF) Growing Convergence Research program (NSF GCR CMMI 1934887) in Materials Life Cycle Management. We also acknowledge using instruments in the Advanced Materials Characterization Lab (AMCL). The use of the NMR facilities at the University of Delaware, founded by the Delaware COBRE program, was supported by a grant from the National Institute of General Medical Sciences – NIGMS (5 P30 GM110758-02) from the National Institutes of Health. The high temperature – gel permeation chromatography experiment and analysis of Pristine LDPE was completed by Dr. Zachary Hinton.

Author Contributions

C.M.O: concept, experiments, analysis, writing. J.S.M.: GPC experiments and analysis for EVOH reactions. J.A.S.: TEM imaging. T.H.E. and L.T.J.K.: advisement on GPC analysis, funding acquisition. D.G.V.: concept, editing, funding acquisition. All authors have reviewed the manuscript.

Declaration of Competing Interest

The authors declare no known competing financial interests or personal relationships that could have appeared to influence the work reported in this paper.

Keywords: Heterogeneous Catalysis • Hydrogenolysis • Multilayer Films • Ruthenium • Waste Valorization

[1] R. Geyer, J. R. Jambeck, K. L. Law, *Science* **2017**, *3,* e1700782.
[2] Z. He, G. Li, J. Chen, Y. Huang, T. An, C. Zhang, *Env. Int.* **2015**, *77*, 85-94.
[3] S. B. Borrelle, J. Ringma, K. L. Law, C. C. Monnahan, L. Lebreton, A. McGivern, E. Murphy, J. Jambeck, G. H. Leonard, M. A. Hilleary, *Science* **2020**, *369*, 1515-1518.
[4] N. Agnes, K. Rajmund, *AARMS* **2016**, *15*, 231-237.
[5] F. P. La Mantia, *Recycling of PVC and mixed plastic waste*, ChemTec Publishing, **1996**.
[6] C. T. d. M. Soares, M. Ek, E. Östmark, M. Gällstedt, S. Karlsson, *Res. Con. Rec.* **2022**, *176*, 105905.
[7] S. Huysveld, K. Ragaert, R. Demets, T. T. Nhu, D. Civancik-Uslu, M. Kusenberg, K. Van Geem, S. De Meester, J. Dewulf, *Was. Man.* **2022**, *152*, 69-79.
[8] D. Lithner, Å. Larsson, G. Dave, *Sci. Tot. Env.* **2011**, *409*, 3309-3324.
[9] N. Alipour, U. W. Gedde, M. S. Hedenqvist, S. Yu, S. Roth, K. Brüning, A. Vieyres, K. Schneider, *Eur. Polym. J.* **2015**, *64*, 36-51.
[10] A.S. Bauer, M. Tacker, I. Uysal-Unalan, R. M. Cruz, T. Varzakas, V. Krauter, *Foods* **2021**, *10*, 2702.
[11] C.H. Huang, J.S. Wu, C.C. Huang, L.-S. Lin, *J. Polym. Res.* **2004**, *11*, 75-83.
[12] T. I. Butler, B. A. Morris, in *Multilayer flexible packaging*, Elsevier, **2016**, pp. 281-310.
[13] T. W. Walker, N. Frelka, Z. Shen, A. K. Chew, J. Banick, S. Grey, M. S. Kim, J. A. Dumesic, R. C. Van Lehn, G. W. Huber, *Sci. Adv.* **2020**, *6*, eaba7599.
[14] K. Kaiser, M. Schmid, M. Schlummer, *Recycling* **2017**, *3*, 1.
[15] A. Rahimi, J. M. García, *Nat. Rev. Chem.* **2017**, *1*, 0046.
[16] J. M. Garcia, M. L. Robertson, *Science* **2017**, *358*, 870-872.
[17] L. Chen, L. C. Meyer, L. Kovarik, D. Meira, X. I. Pereira-Hernandez, H. Shi, K. Khivantsev, O. Y. Gutierrez, J. Szanyi, *ACS Cat.* **2022**, *12*, 4618-4627.
[18] C. Jia, S. Xie, W. Zhang, N. N. Intan, J. Sampath, J. Pfaendtner, H. Lin, *Chem. Catalysis* **2021**, *1*, 437-455.
[19] P. A. Kots, S. Liu, B. C. Vance, C. Wang, J. D. Sheehan, D. G. Vlachos, *ACS Catal.* **2021**, *11*, 8104-8115.
[20] J. E. Rorrer, G. T. Beckham, Y. Román-Leshkov, *JACS Au* **2020**, *1*, 8-12.
[21] J. E. Rorrer, C. Troyano-Valls, G. T. Beckham, Y. Román-Leshkov, *ACS Sustainable Chem. Eng.* **2021**, *9*, 11661-11666.
[22] C. Wang, T. Xie, P. A. Kots, B. C. Vance, K. Yu, P. Kumar, J. Fu, S. Liu, G. Tsilomelekis, E. A. Stach, W. Zheng, D. G. Vlachos, *JACS Au* **2021**, *1*, 1422-1434.
[23] C. Wang, K. Yu, B. Sheludko, T. Xie, P. A. Kots, B. C. Vance, P. Kumar, E. A. Stach, W. Zheng, D. G. Vlachos, *Appl. Catal. B* **2022**, *319*, 121899.

[24] H. K. Chau, Q. P. Nguyen, A. C. Jerdy, D.P. Bui, L. L. Lobban, B. Wang, S. P. Crossley, *ACS Catal.* **2023**, *13*, 1503-1512.
[25] Q. P. Nguyen, L. Lobban, S. Crossley, B. Wang, *Catal. Sci. Technol.* **2023**, *13*, 4477-4488.
[26] T. K. Wu, *J. Polym. Sci. Polym. Phys. Ed.* **1976**, *14*, 343-352.
[27] V. Alvarez, R. Ruseckaite, A. Vázquez, *J. Appl. Polym. Sci.* **2003**, *90*, 3157-3163.
[28] B. Holland, J. Hay, *Polymer* **2001**, *42*, 6775-6783.
[29] S. Krimm, C. Liang, G. Sutherland, *J. Polym. Sci.* **1956**, *22*, 227-247.
[30] J. M. Lagaron, E. Giménez, J. J. Saura, *Polym. Int.* **2001**, *50*, 635-642.
[31] A. Lasagabaster, M. J. Abad, L. Barral, A. Ares, *Euro. Polym. J.* **2006**, *42*, 3121-3132.
[32] Y. Tsuchiya, K. Sumi, *J. Polym. Sci. A-1: Polym. Chem.* **1969**, *7*, 3151-3158.
[33] K. B. Abbås, E. M. Sörvik, *J. Appl. Polym. Sci.* **1973**, *17*, 3577-3594.
[34] J. Ftouni, A. Muñoz-Murillo, A. Goryachev, J. P. Hofmann, E. J. Hensen, L. Lu, C. J. Kiely, P. C. Bruijnincx, B. M. Weckhuysen, *ACS Catal.* **2016**, *6,* 5462-5472.
[35] G. Zhou, X. Tan, Y. Pei, K. Fan, M. Qiao, B. Sun, B. Zong, *ChemCatChem* **2013**, *5*, 2425-2435.
[36] C. Newman, X. Zhou, B. Goundie, I. T. Ghampson, R. A. Pollock, Z. Ross, M. C. Wheeler, R. W. Meulenberg, R. N. Austin, B. G. Frederick, *Appl. Catal. A.* **2014**, *477*, 64-74.
[37] F. Zhang, M. Zeng, R. D. Yappert, J. Sun, Y.-H. Lee, A. M. LaPointe, B. Peters, M. M. Abu-Omar, S. L. Scott, *Science* **2020**, *370*, 437-441.
[38] J. Sun, Y.-H. Lee, R. D. Yappert, A. M. LaPointe, G. W. Coates, B. Peters, M. M. Abu-Omar, S. L. Scott, *Chem* **2023**, *9*, 2318-2336.
[39] S. E. Wanke, P. C. Flynn, *Catal. Rev.* **1975**, *12*, 93-135.
[40] E. H. Kisi, C. Howard, *Key Eng. Mat.* **1998**, *153*, 1-36.
[41] R. Patil, E. Subbarao, *Acta Cryst. A* **1970**, *26*, 535-542.
[42] C. Querini, S. Fung, *Catal. Today* **1997**, *37*, 277-283.
[43] H. Lieske, A. Sárkány, J. Völter, *Appl. Catal.* **1987**, *30*, 69-80.
[44] D. Eisenbach, E. Gallei, *J. Catal.* **1979**, *56*, 377-389.
[45] J. Sun, H. Wang, M. Chen, J. Ye, B. Jiang, J. Wang, Y. Yang, C. Ren, *J. Appl. Polym. Sci.* **2017**, *134*, 44507.
[46] A. Gusev, F. Müller-Plathe, W. Van Gunsteren, U. Suter, *Atom. Mod. Phys. Prop.* **1994**, *116*, 207-247.
[47] J. Sinfelt, in *Advances in catalysis*, Vol. 23, Elsevier, **1973**, pp. 91-119.
[48] M. Salciccioli, W. Yu, M. A. Barteau, J. G. Chen, D. G. Vlachos, *J. Amer. Chem. Soc.* **2011**, *133*, 7996-8004.
[49] B. C. Vance, P. A. Kots, C. Wang, Z. R. Hinton, C. M. Quinn, T. H. Epps III, L. T. Korley, D. G. Vlachos, *Appl. Catal. B* **2021**, *299*, 120483.
[50] H. G. Karge, J. Weitkamp, *Science and Technology* **1999**, *1*.

Entry for the Table of Contents

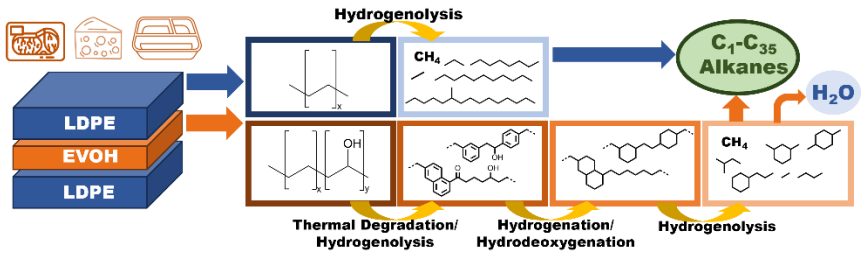

The direct hydroconversion of poly(ethylene-*co*-vinyl alcohol) (EVOH) and polymer blends into alkane products over ruthenium catalysts has been studied. Using a combination of GC, MS, NMR, IR, and GPC, detailed product analysis and catalyst characterization provide fundamental insights into the reaction pathway in the hydrogenolysis of EVOH, which deviates from that of well-studied polyethylene (PE). This approach provides critical insights and outlines a methodology for the hydroconversion of waste multilayer film plastic packaging.